Sapphire mirror for the KAGRA gravitational wave detector

Eiichi Hirose,[1,*] Dan Bajuk,[2] GariLynn Billingsley,[3] Takaaki Kajita,[1] Bob Kestner,[2] Norikatsu Mio,[4] Masatake Ohashi,[1] Bill Reichman,[2] Hiroaki Yamamoto,[3] and Liyuan Zhang[3]

[1] *Institute for Cosmic Ray Research, the University of Tokyo, 5-1-5 Kashiwa-no-ha, Kashiwa, Chiba 277-8582, Japan*
[2] *Zygo Extreme Precision Optics, 3900 Lakeside Drive, Richmond, CA 94806, USA*
[3] *LIGO Laboratory California Institute of Technology, MS 100-36, Pasadena, CA 91125, USA*
[4] *Photon Science Center, the University of Tokyo, 2-11-16 Bunkyo-ku, Hongo, Tokyo 113-8656, Japan*

(Dated: January 17, 2014)

KAGRA, Japanese interferometric gravitational wave detector currently under construction, will employ sapphire test masses for its cryogenic operation. Sapphire has an advantage in its higher thermal conductivity near the operating temperature 20 K compared to fused silica used in other gravitational wave detectors, but there are some uncertain properties for the application such as hardness, optical absorption, and birefringence. We introduce optical design of the test masses and our recent R&D results to address the above properties. Especially, test-polish of sapphire substrate has proven that specifications on the surface are sufficiently met. Recent measurements of absorption and inhomogeneity of refractive index of the sapphire substrate indicate that the other properties are also acceptable to use sapphire crystal as the test masses.

I. INTRODUCTION

There are several ongoing interferometric gravitational wave projects in the world aiming for direct detection of gravitational waves [1–5]. Although each detector's design differs to some extent, they all use the same detection principle that distortion of spacetime will be coupled to phase change in the interferometer through test masses that also work as mirrors. When gravitational waves pass two free-falling test masses, their proper separation oscillates [6, 7]. In reality, test masses are not free-falling but are carefully suspended from a vibration isolation system so that the test masses still can follow geodesics. Since distortion of spacetime is so tiny, the detectors typically employ Fabry-Perot cavities to enhance the phase change. Fundamental noise sources that limit their sensitivity are seismic noise, thermal noise, and quantum noise. Among various techniques to reduce these noises, lowering temperature of mirror-suspension system of the cavities is a way to reduce thermal noise, and KAGRA is the only detector that has taken this path so far (A proof-of-concept cryogenic detector CLIO is in Japan but currently not operational [8].). Since it is necessary that test mass material has high thermal conductivity near the operating temperature 20 K, KAGRA chose sapphire while the other detectors use fused silica. Sapphire, however, has a few disadvantages to fused silica in hardness, absorption, and birefringence. For our application, the effects of birefringence are minimized by choosing C-plane as the mirror surface. Absorption and inhomogeneity of refractive index arise from either impurities or defects in crystal lattice, and these properties completely depend upon quality of the crystal itself. Therefore, we investigated whether sapphire would be applicable to the gravitational wave detector. We address the KAGRA test mass design, results of a test-polish, and properties of a sapphire bulk to discuss the feasibility of using sapphire crystal as the test masses.

* hirose@icrr.u-tokyo.ac.jp

II. FIELD PROPAGATION

If mirrors in a Fabry-Perot cavity were perfectly fabricated, the only losses would be diffraction due to finite size of the mirror surface and transmitted light through ETMs. In reality, there are losses originating from both substrate and coating. They are scattering due to surface aberration which is commonly called either figure or roughness depending on its spatial frequency, scattering of coating, absorption of coating, scattering due to point defects, scratches, sleeks and so on. We do not count bulk absorption as a loss of a cavity. It is hard to predict scattering and absorption from coating layers theoretically, while the other loss sources from the substrate can be treated either numerically or analytically. We briefly explain how to estimate them to determine the specifications below. In the discussion, we assume a coated surface phase map. Propagation of the laser beams is approximated by the paraxial wave equation.

$$\frac{d^2E_t}{dx^2} + \frac{d^2E_t}{dy^2} + 2ik\frac{dE_t}{dz} = 0, \tag{1}$$

where E_t is the slowly varying envelope of a field $E(x,y,z) = exp(-ikz)E_t(x,y,z)$ and k is the wave number of the field. A general solution to the paraxial equation is the Huyghens integral, which is a convolution of the source field envelope $E'_t = E_t(x',y',z')$ and the paraxial diffraction kernel $K(x,y,z)$ [9–11].

$$E_t(x,y,z) = \iint dx'dy'E'_tK(\Delta x, \Delta y, \Delta z) \tag{2}$$

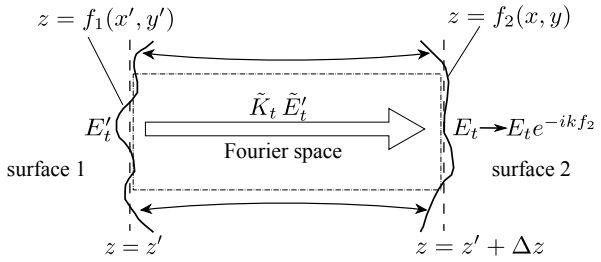

FIG. 1. Field propagation between two mirrors with aberration in a cavity. From $z = z'$ to $z = z' + \Delta z$, FFT technique is used, and phase change due to the arm length Δz, curvature, and surface aberration is taken care of later.

$$K(x, y, z) = \frac{i}{\lambda z} e^{-ik\frac{x^2+y^2}{2z}}, \tag{3}$$

where $\Delta x = x - x'$, $\Delta y = y - y'$, and $\Delta z = z - z'$. In our case, Δz is the arm length, and Δx, Δy are order of the mirror size at most. In Fourier space, this convolution becomes

$$\tilde{E}_t(p, q, z) = \tilde{K}(p, q, \Delta z)\tilde{E}_t(p, q, z'). \tag{4}$$

E_t is given by inverse Fourier transform of $\tilde{E}_t(p, q, z)$.

$$E_t(x, y, z) = \frac{1}{(2\pi)^2} \iint dp\, dq\, e^{-i(px+qy)} \tilde{E}_t(p, q, z). \tag{5}$$

Fast Fourier Transform (FFT) is a technique used to speed up the calculation of the field propagation [12–14]. For non-ideal optics surfaces, we can treat them as deviation from the ideal surfaces. The field propagation inside the cavity is calculated in the following way. First, we apply FFT to convert E'_t to $\tilde{E}'_t(p, q, z')$. Next, we multiply the diffraction kernel $\tilde{K}_t(p, q, \Delta z)$ with $\tilde{E}'_t(p, q, z')$ in Fourier space to get the envelope distribution, $\tilde{E}_t(p, q, \Delta z)$. Then, we inverse FFT $\tilde{E}_t(p, q, \Delta z)$ to have $E_t(x, y, \Delta z)$. Finally, we multiply phase change due to surface profile of the mirror e^{-ikf_i} where $f_i, i = 1, 2$ is deviation from the ideal surface . There are several FFT based packages, and in this analysis a package named *Stationary Interferometer Simulation* (SIS) [13] was used. Spatial resolution of the FFT calculation is normally set as a few mm since the measured phase map of entire mirror surface limits the resolution. For spatial frequencies below the the spatial resolution, we rely on *Golden Rule*, which relates smooth-surface's total integrated scattering (TIS) to roughness in root-mean-square (RMS) σ [15, 16]

$$TIS = \left(\frac{4\pi\sigma}{\lambda}\right)^2 \tag{6}$$

where λ is the wavelength of the laser beam. In order to estimate loss due to point defects, scratches, and sleeks, we treat them as surface aberrations whose area and height are S and h respectively and calculate a perturbed field under some assumptions [17, 18].

TABLE I. Fabry-Perot cavity in KAGRA

arm length	3 km
test mass diameter/thickness	220 mm / 150 mm
radius of curvature (ROC)	1.9 ± 0.0095 km
loss in arm cavity	100 ppm a round trip
transmission ETM/ITM	7 ppm / 0.004
Finesse	~ 1530

TABLE II. loss budget in the KAGRA arm cavity [ppm]

loss sources	KAGRA	aLIGO
diffraction	(1)	1
defects	1+1	(0)
ETM transmission	7	5
figure	30+30	20+20
roughness	5+5	10+10
point scattering	9+9	4+4
absorption	1+1	0.5+0.5

III. DESIGN

KAGRA is a dual-recycled Fabry-Perot Michelson interferometer [19], and the main parameters are summarized in TABLE I. Design of test masses is then to deliver the cavity by managing several loss sources inside. The size of the test mass is limited by an available high quality C-axis sapphire crystal in terms of purity, absorption, and homogeneity. The crystal is grown along the A-axis with a bigger size [20], but our choice to use C-plane as mirror surface results in the size in TABLE I. Of course, a larger size is preferred, in order to reduce thermal noise. The transmittance of the end test mass (ETM) will be counted as a loss. TABLE II shows the planned loss budget inside the cavity. For comparison, advanced LIGO's case is also listed [18, 21]. Diffraction is a loss purely due to finite size of the mirror, and for KAGRA it is two orders of magnitude smaller than 1 ppm. Scattering and absorption from coating layers really depend on quality of coating technology, so we set the numbers after discussion with a couple of coaters. We are planning to do coating tests with them to see if our loss budget is achievable. All that is left is how we break the rest down into defects, figure, and roughness. SIS introduced in the previous section is able to generate random surfaces with a RMS roughness both inside and outside clear aperture. We investigated a parameter space that includes clear aperture, RMS error inside, and RMS error outside to see how much loss is generated in SIS with one hundred pairs of randomly generated surfaces representing two mirrors. After trial and error, we decided to set the clear aperture as 140 mm in diameter. FIG. 2 shows distribution of loss in the arm cavity due to surface aberration while FIG. 3 shows accumulated

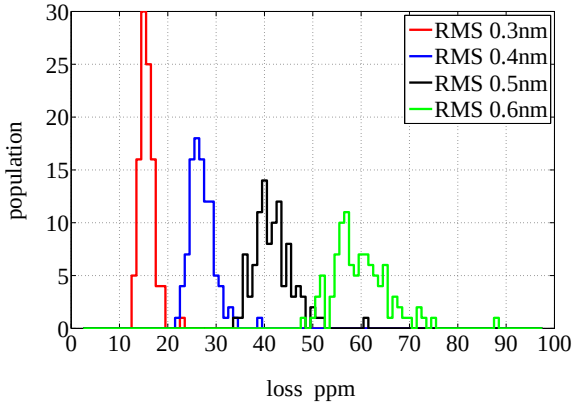

FIG. 2. Distribution of loss calculated by *SIS* due to randomly generated surfaces' aberration with a certain RMS. In each RMS, 100 pairs of surfaces were generated to make a Fabry-Perot cavity for the calculation.

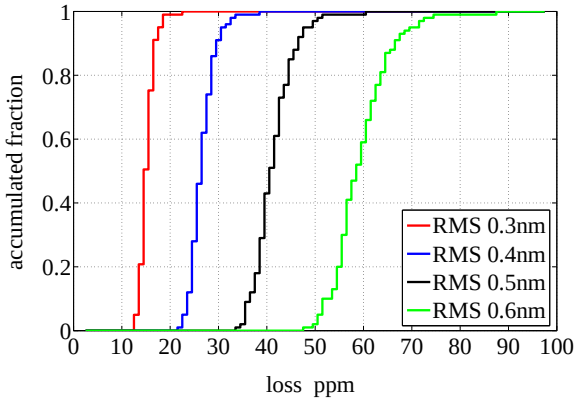

FIG. 3. Accumulated fraction of loss for each RMS in FIG. 2. This shows how much fraction of population is below a certain loss. For RMS=0.5 nm, 98% of the calculated results is below 50 ppm.

fraction that gives us how much fraction exists below a certain loss. We set RMS 2 nm outside the clear aperture for all cases. These results convinced us to have RMS 0.5 nm inside the clear aperture since it will be safe to say that loss due to figure error in the cavity is likely to be below 50 ppm. In this case, higher order mode (HOM) fraction to the power inside the cavity is about 0.07 ppm. Adding 20 % margin results in 60 ppm loss in the budget for figure error. This decision leaves 12 ppm for micro roughness and defects (In aLIGO, defects are included under roughness). We set RMS 0.16 nm for high spatial frequency error above 1 mm^{-1}, which should correspond to 3.6 ppm according to the equation (6). We count this loss as 5 ppm per mirror to get about 40 % margin (10 ppm total loss in the cavity). For simplicity, we count defects of radius greater than 2 μm as point defects and defects of radius greater than 25 μm as scratches. For defects of radius smaller than 2 μm is controlled by defect's density. For instance, a defect with radius 2 μm, depth 20 nm, and density 0.25, gives loss of 0.06 ppm. As for point like defects of radius 25 μm, the loss will be 0.02 ppm. We set the total number of those point defects less than 10 inside 100 mm diameter, and 50 over the entire surface, which corresponds to loss of 0.4 ppm. For scratches, 0.5 ppm corresponds to the total area 1.5×10^4 μm^2 that sets the upper limit over the entire surface area. Since the beam power is higher at central region, we set 2000 μm^2 scratches inside 100 m^2 diameter, which corresponds to loss of 0.064 ppm.

IV. TEST POLISH

In the previous section, we described how to break the total cavity loss into several loss sources such as surface aberration. Irregularities of surface profile is directly related to specification of polishing, and we therefore investigated whether those specifications in figure error, roughness, and surface quality such as point defects, scratches, and sleeks could be achieved in reality. We performed a test-polish study with two sapphire substrates fabricated by GT Advanced Technologies as a pathfinder. One is their highest grade crystal whose diameter is 100 mm while the other is a 200 mm-diameter standard grade one. The test-polish was performed at Zygo Extreme Precision Optics (Zygo EPO) [22], and the results are summarized in TABLE. III. The first six

TABLE III. results of test-polish

	ZYGO	CALTECH	Spec's
@ 140 mm diameter			
Radius m	2001.90	2004.61	2000 ± 10
figure RMS nm	0.24	0.21	0.5
astigmatism $Z_{2,2}$	-0.41	-0.13	3
astigmatism $Z_{2,-2}$	0.26	0.27	3
@ 180 mm diameter			
Radius m	2003.46	2006.34	-
figure RMS nm	0.48	0.45	-
astigmatism $Z_{2,2}$	-0.68	-0.30	-
astigmatism $Z_{2,-2}$	0.45	0.29	-
@ HSF errors			
1-750 mm^{-1} nm	0.11	-	0.16
@ Surface Quality (defects)			
area @ 100 mm μm^2	0	-	2000
area @ 180 mm μm^2	14200	-	15000
point $> 2\mu m$ @ 100 mm	0	-	10
point $> 2\mu m$ @ 200 mm	0	-	82
point density $< 2\mu m$ mm^{-2}	0	-	0.25

Zernike terms have been subtracted for figure RMS and high spatial frequency (HSF) roughness RMS. This operation is justified since these terms will disappear when mirrors are aligned to form a cavity. Radius of curvature (ROC) and figure error were independently measured at both Zygo EPO and Caltech and most of the two measurements agree well except ROC. FIG. 4 shows phase map of the polished surface, measured at Zygo EPO. The surface was characterized to have the radius and figure error using a full aperture interferometer relative to a 12 inch transmission sphere whose radius is 2 km. We chose 2 km intentionally instead of 1.9 km for convenience. The transmission sphere was calibrated to a high precision flat, and estimated accuracy for figure, radius, and astigmatism should be 0.15 nm, ±5 m, and 0.2 nm respectively [23]. Sub-aperture interferometric measurement technique named *Phase Measuring Microscope* (PMM) was used to measure high spatial frequency error of the surface using 2.5x and 50x microscope objectives. PMM is calibrated semi-annually for each objective using a commercial target with NIST traceable certifications. FIG. 5 shows typical high spatial frequency error maps by PMM. The estimated accuracy of this high spatial frequency error should be less than RMS 0.05 nm. The surface was visually inspected for defects such as points, scratches, sleeks, and so on with both room light and a 150 W fiber light. FIG. 6 shows the power spectral density (PSD) of the polished surfaces of both 100 mm and 200 mm substrates. The Zygo report for 200mm substrate is a composite plot of three measurements, figure, PMM2.5x, and PMM50x while 100mm is one from two PMM measurements only. For low spatial frequency part (figure), two independent measurements done at Zygo and Caltech are in the plot and they agree fairly well. For comparison, fused silica data is on the plot, one of advanced LIGO's test mass data. In this frequency band, fused silica is better there. We believe this is not a fundamental disadvantage of sapphire but it just takes longer in polishing mainly because of hardness of the material. For high spatial frequency region, the high grade 100 mm sapphire's result is better than both the standard 200 mm sapphire and fused silica. Overall, we did not see disadvantages in terms of PSD in spatial frequencies we explored. A model that gives about RMS 0.27 nm when integrating from 0.01 mm^{-1} to 1 mm^{-1} is above our results, which makes sense given measured RMS values.

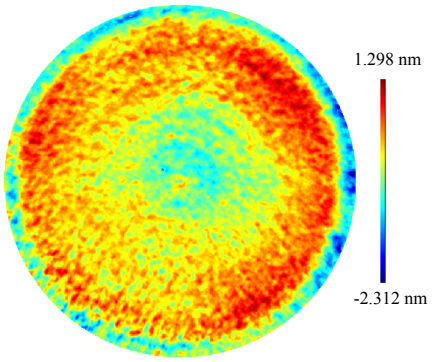

FIG. 4. Phase map of figure error (low spatial frequency) measured at Zygo EPO (200 mm sapphire). The aperture size is 180 mm here. RMS is 0.48 nm over the diameter and 0.24 nm over 140 mm. Figure measurement done at Caltech using a different Fizeau interferometer showed almost the same results.

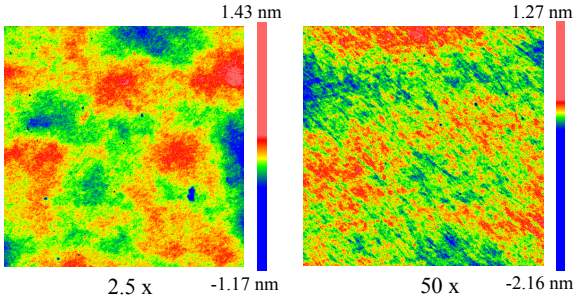

FIG. 5. Phase maps of high spatial frequency (HSF) error measured at Zygo EPO (100 mm sapphire) using PMM. The left is the result by 2.5x while the right is one by 50x. Size of the map shown here is 4.9 mm × 4.9 mm (left) and 0.5 mm × 0.5 mm (right), respectively.

V. CRYSTAL PROPERTIES

In this section, we discuss absorption and inhomogeneity of refractive index in 100 mm-diameter sapphire crystal used in the test polish study. Absorption coefficient needs to be smaller than 50 ppm/cm in order for test masses to be cooled down to 20 K by the cryostat. Using Photothermal Common-path Interferometer (PCI) technique [24], we measured absorption of the bulk over 50 mm central aperture. The interaction points were set 2 mm from a surface and data was taken every 1 mm step over the aperture to count the total number 1961. FIG. 7 shows a phase map taken in this method. The mean value is 43.4 ppm/cm and the standard deviation is 8.0 ppm/cm. Due to nature of relative measurement technique, there is some uncertainty about the absolute value, but the system's noise floor should be about RMS 2 ppm/cm. There is a clear line where absorption is higher than the other region. There is a clear correlation between absorption and distribution of refractive index in the bulk. The region of high absorption in FIG. 7 lines up where dn is higher. We think of this as something related to lattice defect, and we are planning to work together with the crystal maker to tune some parameters in fabrication process for lower absorption substrates. Inhomogeneity of refractive index is very important especially for Input Test Mass (ITM). If index of refraction is not homogeneous inside the bulk, the ideal wavefront profile will be degraded to generate higher order modes

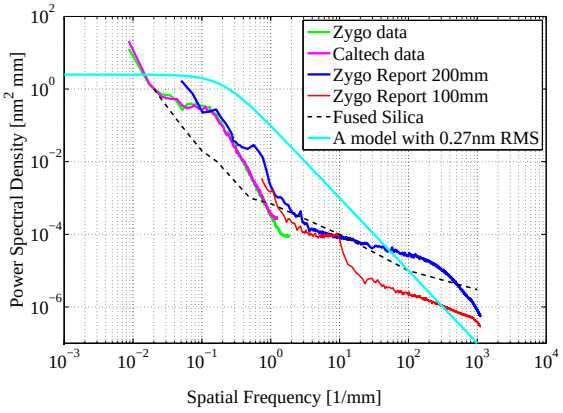

FIG. 6. PSD plot of both 200 mm and 100 mm sapphire substrates. Zygo report for 200 mm substrate is a composite plot of three measurements, figure, PMM2.5x, and PMM50x while 100 mm is one from only two PMM measurements only. For low spatial frequency part (figure), two independent measurements done at Zygo and Caltech agree fairly well. For comparison, fused silica data is in the plot, which is one of advanced LIGO's test mass data. We did not find disadvantages in terms of PSD. A model that gives 0.27 nm in RMS when integrating from 0.01 mm^{-1} to 1 mm^{-1} is above our results.

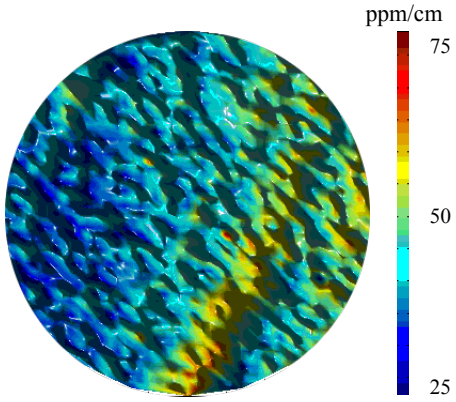

FIG. 7. Absorption of 100 mm sapphire substrate in ppm/cm. The aperture size is 50 mm and the interaction point is 2 mm from the surface. There is a line where absorption is higher than the other regions.

when the beams propagate through it. There is a technique to compensate this inhomogeneity of optical path difference, typically by polishing the back surface. We measured inhomogeneity of refractive index of the sapphire bulk using the same full aperture interferometer at Caltech used to measure figure of 200 mm-diameter sapphire. In order to kill effect of surface profile of the substrate, we measured side 1, side 2, and side 2 through side 1 [25]. FIG. 9 shows a phase map of inhomogene-

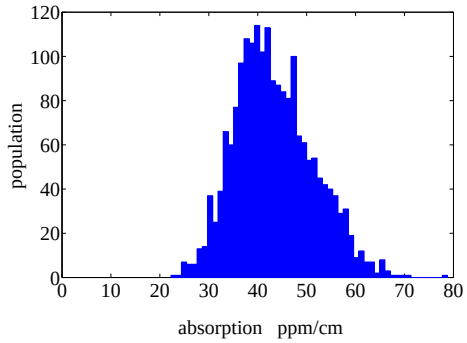

FIG. 8. Distribution of absorption in FIG. 7. The mean is 43.4 ppm/cm and the standard deviation is 8.0 ppm/cm.

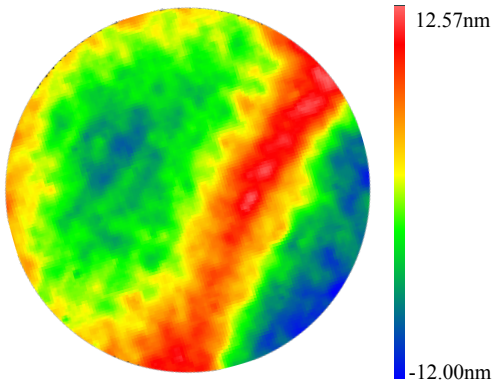

FIG. 9. Phase map of homogeneity of refractive index. The unit is nm since data is product $dn \times thickness$. We measured three wavefront data, side 1, side 2, and side 2 through side 1. The last one contains information of refractive index of the bulk, and carefully subtracted information of both side 1 and side 2. Then, terms up to power term were subtracted to bring the inhomogeneity to light. This is what will be left even if we have a spherical backsurface profile to compensate the inhomogeneity and the level is about 8×10^{-8} after dividing by the thickness.

ity $dnxt$ of the bulk over 50 mm aperture, where dn and t are variation of refractive index and thickness of the bulk, respectively. There is a similar line to one in 7 in the map where deviation is higher than the other region. After removing piston, tilt, and power terms, we had PV 24.57 nm and RMS 4.997 nm. Given the substrate is 60 mm thick, this corresponds to $dn = 8 \times 10^{-8}$ over the aperture.

VI. DISCUSSION

Although we are confident that the sapphire substrate can be polished to meet our surface specifications, we

do still need to check whether coating specifications such as uniformity, scattering, and absorption are satisfied on sapphire substrates. Our current plan is to use multi-layered dielectric coating of SiO_2 and Ta_2O_5, and we have to make sure that optical properties are acceptable and polished surface is actually preserved after coating in terms of radius of curvature, figure error, and so on. Otherwise, we would need to feedback the specifications of polishing to have smaller errors. A literature introduced a very low loss coating on a 30 mm diameter sapphire substrate [26], and Cryogenic Laser Interferometer Observatory (CLIO) already demonstrated a loss less than 100 ppm in the arm cavity whose test masses are 100 mm-diameter sapphire mirrors [27]. We are planning to do a test-coating study using the substrates we described here to see if our low loss coating specifications are feasible. For the inhomogeneity of refractive index, we think at least that we are able to reduce it by polishing the back surface to compensate up to power term as we processed data in the previous section. It is even possible to remove the structure due to lattice distortion in FIG. 9 by a technique called *Ion Beam Figuring* (IBF). However, if the origin of the structure is deep inside the substrate, the phase map coming out of the back surface will be sensitive to alignment of the optic. And, considering a fact that test masses will move all the time, we would like to have the inhomogeneity as small as possible. Because of the correlation between absorption and inhomogeneity of refractive index, we believe this direction should reduce absorption level of substrate. Therefore, it is essential to study both structure of refractive index and absorption inside sapphire bulk to give us a hint for better crystal fabrication. According to discussion with the crystal maker, there are several parameters that can be tuned to control growth of their sapphire crystal. If inhomogeneity of refractive index were applied to one of ITMs in the gravitational wave detector, the optical path difference (OPD) generated through the ITM δx would cause a fractional reduction of detector's sensitivity by $(k\delta x)^2 \sim 5 \times 10^{-3}$ [26]. We need a full interferometer simulation with real data for more accurate discussion. Of course, the effect is not so small but it is fair to say that the effect is not disastrous. Another issue we should mention here is that all metrology are done in room temperature conditions while test masses will be cooled down to 20 K and suspended from a cryogenic suspension system. Therefore, we need to analyze effect of the environmental difference between lab and operating conditions. These issues are very important for performance of the detector and left for future works.

VII. CONCLUSION

We addressed optical design of cryogenic mirror for the KAGRA gravitational wave detector. We performed a test-polish with C-axis sapphire substrates and demonstrated that the specifications were satisfied. It turned out that the high quality sapphire crystal would be usable as the test masses even if absorption and inhomogeneity of refractive index of real test mass crystal were equal to those of the bulk we tested. In order to have smaller absorption and more homogeneous index of refraction, we need a better understanding of sapphire crystal. Although we have some experience in coating on sapphire substrates, a study of test-coating is planned to check whether our specifications are satisfied in reality.

ACKNOWLEDGMENTS

We are grateful for the financial support from Leading-edge Research Infrastructure Program funded by the Ministry of Education, Culture, Sports, Science and Technology (MEXT) in Japan. The LIGO Observatories were constructed by the California Institute of Technology and Massachusetts Institute of Technology with funding from the NSF under cooperative agreement PHY-9210038. The LIGO Laboratory operates under cooperative agreement PHY-0328418. We would like to thank our colleagues in both KAGRA collaboration and the LIGO Scientific Collaboration (LSC). This paper has document numbers JGW-P1302017 and LIGO-P1400005.

[1] LIGO, `http://www.ligo.caltech.edu/`.
[2] VIRGO, `https://wwwcascina.virgo.infn.it/`.
[3] GEO600, `http://www.geo600.org/`.
[4] KAGRA, `http://gwcenter.icrr.u-tokyo.ac.jp/`.
[5] Einstein Telescope, `http://www.et-gw.eu/`.
[6] C. W. Misner, K. S. Thorne, and J. A. Wheeler, *Gravitation* (Freeman, 1973).
[7] P. R. Saulson, *Fundamentals of Interferometric Gravitational Wave Detectors* (World Scientific, 1994).
[8] S. Miyoki, T. Uchiyama, K. Yamamoto, M. Ohashi, K. Kuroda, T. Akutsu, S. Kamagasako, N. Nakagawa, M. Tokunari, K. Kasahara, S. Telada, T. Tomaru, T. Suzuki, N. Sato, T. Shintomi, T. Haruyama, A. Yamamoto, D. Tatsumi, M. Ando, A. Araya, A. Takamori, S. Takemoto, H. Momose, H. Hayakawa, W. Morii, and J. Akamatsu, Class. Quantum Grav. **23**, S231 (2006).
[9] M. Born and E. Wolf, *Principles of Optics* (Cambridge University Press, 2002).
[10] A. E. Siegman, *Lasers* (University Science Books, 1986).
[11] P. C. D. Hobbs, *Building Electro-Optical Systems* (Wiley, 2009).
[12] J.-Y. Vinet, P. Hello, C. Man, and A. Brillet, J. Phys. I France **2**, 1287 (1992).
[13] Hiroaki Yamamoto, *SIS (Stationary Interferometer Simulation) maual* (LIGO-T070039-v7, 2011).

[14] T. Tomaru, S. Miyoki, M. Ohashi, K. Kuroda, T. Uchiyama, T. Suzuki, A. Yamamoto, T. Shintomi, A. Ueda, D. Tatsumi, S. Sato, K. Arai, K. W. Masaki Ando, K. Nakamura, M. Watanabe, K. Ito, I. Kataoka, H. Yamamoto, B. Bochner, and Y. Hefetz, Applied Optics **41 No 28**, 5913 (2002).

[15] J. Bennett and L. Mattsson, *Introduction to Surface Roughness and Scattering, Second Edition* (Optical Society of America, 1999).

[16] J. C. Stover, *Optical scattering: measurement and analysis, 2nd ed* (SPIE - The International Societ for Optical Enginering, 1995).

[17] Hiroaki Yamamoto, *Effect of amall size anomalies in a FP cavity* (LIGO-T1000154-v5, 2010).

[18] Hiroaki Yamamoto, *Advanced LIGO Optics and interferometer performance* (LIGO-G1300398-v2, 2013).

[19] Y. Aso, Y. Michimura, K. Somiya, M. Ando, O. Miyakawa, T. Sekiguchi, D. Tatsumi, and H. Yamamoto, Physical Review D **88**, 043007 (2013).

[20] C. P. Khattak, P. J. Guggenheim, and F. Schmid, Proc SPIE **5078**, 47 (2003).

[21] H. Yamamoto, O plus E **34**, 618 (2012).

[22] Bill Reichman and Robert Kestner, *200mm Pathfinder Result Summary* (Zygo ATP, 2013).

[23] Bill Reichman and Robert Kestner, *KAGRA 200mm Pathfinder* (Zygo ATP, 2013).

[24] Liyuan Zhang and GariLynn Billingsley and Margot Phelps, *QA Test Procedure for aLIGO COC* (LIGO-E1000863-v2, 2011).

[25] B. F. Oreb, A. J. Leistner, G. Billingsley, W. P. Kells, and J. Camp, SPIE **4451**, 414 (2001).

[26] D. G. Blair, M. Notcutt, C. T. Taylor, E. K. Wong, C. Walsh, A. Leistner, J. Seckold, J.-M. Mackowski, P. Ganau, C. Michel, and L. Pinard, Applied Optics **36 No.1**, 337 (1997).

[27] S. Miyoki, Private communication (2013).